DOI: 10.1016/S1872-5813(21)60127-5

Catalytic pyrolysis of sugarcane bagasse by zeolite catalyst for the production of multi-walled carbon nanotubes

ABOUL-ENEIN Ateyya A.[1,2,*], AWADALLAH Ahmed E.[1,2],
EL-DESOUKI Doaa S.[1], ABOUL-GHEIT Noha A.K.[1]
(1. *Process Development Division*, *Egyptian Petroleum Research Institute*, *Cairo* 11727, *Egypt*;
2. *EPRI-Nanotechnology Center*, *Egyptian Petroleum Research Institute*, *Cairo* 11727 , *Egypt*)

Abstract: Recently, the disposal of waste by beneficial and environmentally friendly methods has attracted great attention. In this work, we have studied the production of high-value carbon nanotubes (CNTs) which have remarkable applications by catalytic pyrolysis of sugarcane bagasse (SCB) as an agricultural waste using a two-stage process. Various reaction factors including the effects of zeolite types (HZSM-5, HMOR, and HY), pyrolysis temperatures (450−700 °C), and SCB/ZSM-5 ratios (3−12) on SCB pyrolysis were investigated to generate CNTs from pyrolysis products. A Co-Mo/MgO catalyst was used for growing CNTs via the decomposition of pyrolysis products. The morphological structure and quality of CNTs were characterized using TEM and Raman spectroscopy, while the fresh Co-Mo/MgO catalyst was characterized by XRD and TPR analyses. The results showed that zeolite type, pyrolysis temperature, and SCB/ZSM-5 ratio had significant effects on the CNTs yield. The optimum carbon yield (24.9%) was achieved using the HZSM-5 catalyst at the pyrolysis temperature of 500 °C and with the SCB/ZSM-5 ratio of 6. TEM observations confirmed the growth of bamboo-like carbon nanotubes (BCNTs) and carbon nano-onions (CNOs) in different proportions according to the reaction parameters. Also, CNTs with the largest diameter distribution range (7−76 nm) were produced using the SCB/ZSM-5 ratio of 6. Raman spectra demonstrated the production of high-quality CNTs under all studied conditions.

Key words: carbon nanotubes; Co-Mo/MgO; pyrolysis; sugarcane bagasse; ZSM-5 zeolite
CLC number: O643.3 **Document code:** A

Biomass is sustainable and renewable organic material that can be used as feedstock to generate a broad variety of high-value products[1−4]. Generally, low-efficiency energy is produced along with serious air pollution by the uncontrolled combustion of biomass waste. Pyrolysis is defined as the degradation of a biomass feedstock by the influence of heat in a non-oxygenated environment to generate bio-oil (liquid), bio-char (solid), and non-condensable gases[5]. Bio-oil contains a variety of organic compounds that have a large amount of oxygen[6]. Solid bio-char mainly contains carbon, plus some oxygen, hydrogen, and inorganic ash. Bio-char has a wide range of applications due to its interesting physicochemical characteristics[7, 8]. Sugarcane is the largest agricultural crop that can be used to generate sugar and bioethanol. Mature stalks consist of 11%−16% fiber, 12%−16% soluble sugars, 2%−3% non-sugars, and 63%−73% water[9]. A large quantity of fibrous by-product known as bagasse (agro-waste) is produced from sugarcane after extracting the juice. Approximately 270 kg of dry bagasse is produced per ton of sugarcane[10]. SCB consists of cellulose (40%−50%), hemicellulose (20%−30%), lignin (20%−25%), and ash (1.5%−3.0%)[11, 12]. Moreover, SCB has a high energy content, which meets the energy requirements of developing countries. However, burning bagasse to obtain thermal energy causes many environmental problems. Pyrolysis vapors (bio-oil) and gases generated from SCB can be used as a carbon source to form carbon nanomaterials (CNMs). The production of CNMs from agricultural waste is attracting more attention worldwide due to their high carbon content, renewable nature, low price, and abundance.

CNTs, carbon nanofibers (CNFs), and graphene are the most in-demand CNMs nowadays because of their unique properties and wide applications[13−17]. Among all CNMs, CNTs are the most widely researched

Received: 2021-03-17; Revised: 2021-05-14

* Corresponding author. E-mail: ateyya_epri2007@yahoo.com.

The project was supported by the Science and Technology Development Fund (STDF) in Egypt (34830).
本文的英文电子版由 Elsevier 出版社在 ScienceDirect 上出版 (http://www.sciencedirect.com/science/journal/18725813)

material in the areas of synthesis, properties, and applications. The most popular methods for generating CNTs are arc discharge[18], laser vaporization[19], and chemical vapor deposition (CVD)[20 – 22]. The catalyst plays a vital role in the growth of CNTs by the CVD method. The most widely used catalysts for the production of CNTs are based on transition metals, especially Fe, Co, or Ni[23 – 25]. It is possible to convert lignocellulosic biomass into various C-containing products, such as CO_x-gases, aliphatic and aromatic hydrocarbons (CH_4, C_2H_4, benzene, toluene, and xylene), and their related derivatives (CH_3OH and phenol)[3, 26], which can be used as a carbon source for the formation of CNTs. Various research papers have been published on the synthesis of CNMs from different biomass feedstocks. Liu et al[27] tested the in-situ synthesis of CNFs by pyrolysis of fir sawdust preloaded with $FeCl_3$ as the raw material for an iron catalyst. They concluded that a high yield of CNFs was obtained after rapid pyrolysis of oven-dried biomass wastes. They suggested that $FeCl_3$ could enhance the decomposition of lignocellulosic biomass into light hydrocarbons, such as CH_4, C_2H_4, and C_2H_2, which were then deposited onto the iron species to form CNFs. Thompson et al[28] applied a facile one-step method for the synthesis of straight and BCNTs by pyrolysis of softwood sawdust loaded with iron nitrate at 800 °C. Bernd et al[29] studied the synthesis of CNMs (CNTs/CNFs) via pyrolysis of wood sawdust mixed with commercial zinc as a reducing agent, calcite as a bed material, and ferrocene or Fe/Mo/MgO as a catalyst, arranged in a vertical tubular reactor. The obtained CNTs/CNFs samples grew in different sizes and had many defects. Alves et al[30] used a pyrolysis-catalysis process to prepare CNMs from SCB or corn-derived distillers dried grains with solubles (DDGS) at temperatures of 600 and 1000 °C. The growth of CNMs was achieved by CVD of the pyrolyzates on type 304 stainless steel screens as a catalyst. They concluded that long and straight multi-walled CNTs (MWCNTs) with diameters ranging from 20 to 50 nm were generated from bagasse. However, a rope-like carbon nanostructure with diameters ranging from 100 to 300 nm was generated from DDGS.

Based on our latest knowledge, the production of CNTs by catalytic pyrolysis of agro-waste in a semi-batch reactor has not been studied yet. Consequently, the main objective of this work is to determine the optimal process parameters for the synthesis of CNTs by catalytic pyrolysis of SCBs in a semi-batch reactor. The catalytic pyrolysis of SCB was first performed on a zeolite catalyst in a semi-batch reactor to generate carbon-rich pyrolysis products, which were subsequently used for the growth of CNTs on the Co-Mo/MgO catalyst. The effects of zeolite type, pyrolysis temperature, and SCB/ZSM-5 ratio on SCB pyrolysis have been studied to generate CNTs from pyrolysis products. The relationship between the process parameters and the type, quantity, and quality of the produced CNMs was monitored.

1 Experimental

1.1 Biomass feedstock preparation

SCB was collected from the local Egyptian market, dried overnight in the presence of air at 130 °C, and then cut into small parts with dimensions of ~3 mm× 3 mm. The dried SCB was successively heated (torrefied) at 200 °C for 1 h and at 300 °C for 0.5 h under 250 mL/min N_2 gas flow rate to reduce oxygen and moisture content.

1.2 Catalysts preparation

Various zeolite catalysts (Alfa Aesar) including NH_4-ZSM-5 (Si/Al = 23), NH_4-MOR (Si/Al = 20), and NH_4-Y (Si/Al = 5.2) were purchased in the powder form. These zeolites were calcined at 500 °C for 3 h in a muffle furnace in the presence of air to obtain their acidic form before being used in the catalytic pyrolysis of bagasse.

The Co-Mo/MgO catalyst containing 45% Co and 5% Mo was prepared using the conventional co-impregnation method. The estimated quantities of $Co(NO_3)_2{\cdot}6H_2O$ and $(NH_4)_6Mo_7O_{24}{\cdot}4H_2O$ (Sigma-Aldrich) were dissolved in a limited volume of deionized water. Thereafter, the calculated amount of MgO support (CARLO ERBA reagents) was added to the solution under stirring, and then gently heated to evaporate the excess water. This mixture was dried overnight at 110 °C and then calcined in a muffle furnace at 600 °C for 4 h to obtain the final oxide form of the Co-Mo/MgO catalyst.

1.3 Apparatus and procedure

The production of CNTs was carried out by catalytic pyrolysis of SCB using a simple two-stage process. Figure 1 shows the system used to convert SCB to CNTs. As shown in Figure 1, SCB pyrolysis was performed in a semi-batch reactor (outer diameter =

4 cm and length = 90 cm), while the CNTs growth was carried out in a horizontal reactor (outer diameter = 2.5 cm and length = 100 cm). The temperatures of these reactors were controlled using two separate furnaces. The two reactors were connected together by a small glass tube (0.6 cm in diameter and 12 cm in length) to transfer the pyrolysis products from reactor I to reactor II. In detail, the semi-batch reactor was filled with a mixture of pre-treated bagasse and zeolite catalyst and heated to the desired temperature at a heating rate of 20 °C/min. Exactly 0.5 g of Co-Mo/MgO, as the growth catalyst for CNTs, was inserted in the middle of the horizontal reactor. Various factors were studied for the synthesis of CNTs by catalytic pyrolysis of SCB. The effects of different zeolite catalysts, including HZSM-5, HMOR, and HY on bagasse pyrolysis were investigated at 500 °C by mixing 2 g of each zeolite catalyst with 24 g of the pretreated SCB. Besides, the impact of pyrolysis temperature (450−700 °C) on bagasse pyrolysis was studied using the same previous amounts of bagasse and HZSM-5. To study the generation of CNTs at different SCB/ZSM-5 ratios (3, 6, 9, and 12), pyrolysis of various amounts of bagasse was performed using a fixed amount of ZSM-5 at 500 °C. All studied parameters were performed at a constant growth temperature of 700 °C. Firstly, an *in-situ* reduction of the Co-Mo/MgO catalyst was performed at 600 °C for 1 h under a pure H_2 flow of 60 mL/min, to obtain the active form of the catalyst. Then, the H_2 gas flow was stopped and the catalyst temperature was increased to 700 °C under N_2 flow. At this moment, the semi-batch reactor was heated to the required temperature to convert SCB to carbon-rich volatile products, which were subsequently transferred to the horizontal reactor to form CNTs on the Co-Mo/MgO catalyst. Both the bagasse pyrolysis and CNTs growth in this process continued for 1 h. Finally, the carbon products were cooled to room temperature under N_2 gas flow. At all the studied parameters, the yields of the pyrolysis products were calculated according to the initial mass of the treated SCB. Also, the carbon yield was determined according to the mass of the reduced Co-Mo/MgO catalyst using the following equation:

$$\text{Carbon yield}(\%) = \frac{M_{\text{tot}} - M_{\text{cat}}}{M_{\text{cat}}} \times 100 \quad (1)$$

Where, M_{tot} is the mass of the deposited carbon product, and M_{cat} is the mass of the reduced Co-Mo/MgO catalyst.

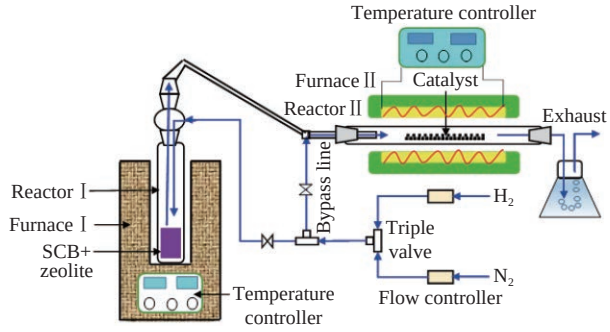

Figure 1　Schematic diagram of the system used to convert SCB to CNTs

1.4　Characterization Techniques

X-ray diffraction (XRD) analysis was carried out using a PANalytical XPert PRO diffractometer to evaluate the crystalline structure of the freshly calcined Co-Mo/MgO catalyst and also the zeolite catalysts. The crystallite sizes of all the catalysts were calculated using the well-known Debye-Scherrer equation ($L_c = k\lambda/\beta \cos\theta$).

The reducibility of the freshly calcined Co-Mo/MgO catalyst was evaluated via performing a temperature-programmed reduction (TPR) experiment. A BELCAT-II catalyst analyzer (BEL Inc., Japan) was used to implement TPR analysis at temperatures from 100 to 1000 °C with 5% H_2 in Ar gas.

Transmission electron microscopy (TEM) analysis of the carbon product was performed at 200 kV using the model JEM-200CX of JEOL, Japan. Small droplets of carbon suspended in ethanol were loaded onto a copper grid and then introduced into a microscope to be amplified.

The SENTERRA Dispersive Raman Microscope (Bruker) equipped with a diode Nd YAG laser (λ = 532 nm) was used to detect Raman spectra of CNTs at room temperature.

The temperature-programmed ammonia desorption test (NH_3-TPD) was conducted using the BELCAT-II chemisorption device (BEL Inc., Japan) to assess the acidic nature of zeolites. Initially, the zeolite catalyst was activated by heating at 300 °C for 2 h. TPD data were obtained at a heating rate of 5 °C/min under a helium flow.

2　Results and discussion

2.1　Characterization of the fresh catalysts

XRD analysis is performed to study the crystal structure of the fresh catalysts used in this study. The XRD pattern of the calcined Co-Mo/MgO catalyst is

displayed in Figure 2(a). As illustrated, various diffraction peaks are detected at 2θ values of 18.7°, 31.2°, 36.7°, 38.3°, 44.7°, 59.2°, 65.1°, and 76.7°, which corresponding to the crystalline structure of Co_3O_4 species[31]. Also, several peaks related to MgO are observed in the diffraction pattern. There are no peaks for CoO and MoO_x species (MoO_3, $CoMoO_4$, and $MgMoO_4$), indicating the complete interaction of MoO_3 with both CoO and MgO to form small-sized particles of highly dispersed $CoMoO_4$ and $MgMoO_4$ phases. This result is compatible with our previous works, in which no diffraction peaks related to Mo were observed in Co or Fe-based catalysts with low Mo concentrations[32, 33]. These results demonstrate the presence of free Co_3O_4 species on the surface of MgO, as well as the existence of $CoMoO_4$ and $MgMoO_4$ in the form of small size particles. Using XRD data, the average crystallite size determined from the Scherrer equation for the 45% Co-5% Mo/MgO catalyst is 25.8 nm. Figure 2(b) displays the TPR results of the freshly prepared Co-Mo/MgO catalyst. The TPR profile illustrates two strong reduction peaks at temperatures between 200 and 1000 °C. The low-temperature peak (415 °C) indicates the complete reduction of non-interacted Co_3O_4 species to form the cobalt metal[34, 35]. Meanwhile, the broad peak at temperatures between 450 and 1000 °C is related to the reduction of mixed oxides species such as Co_2MgO_4, $MgMoO_4$, and $CoMoO_4$[36−39]. The TPR analysis indicates that the Co-Mo/MgO catalyst is composed of unreacted Co_3O_4 as well as mixed oxide species.

XRD patterns for all zeolite catalysts are shown in Figure 2(c). Obviously, the characteristic peaks of HZSM-5, HMOR, and HY are observed. The XRD pattern of HZSM-5 shows distinct diffraction peaks at 2θ values in the ranges of 7°−10° and 22°−25°[40, 41]. The pattern of HY is similar to that previously reported in the literature[42]. Using XRD data, the average crystallite size for HZSM-5, HMOR, and HY are 43, 41, and 51 nm, respectively. Figure 2(d) shows the NH_3-TPD profiles of all zeolite catalysts used for catalytic pyrolysis of SCB. Two strong desorption peaks are observed in the profiles of all zeolites, indicating the presence of large numbers of acid sites. For each zeolite catalyst, the peaks observed at both low and high temperatures are due to ammonia gas desorption from the weak and strong acid sites, respectively[43−45]. Generally, the presence of strong acid sites implies the existence of bridging hydroxyl groups between the Si and Al atoms (Brönsted sites) in the zeolite framework, whereas the presence of weak acid sites is due to the silanol groups or non-framework aluminum species[46−48].

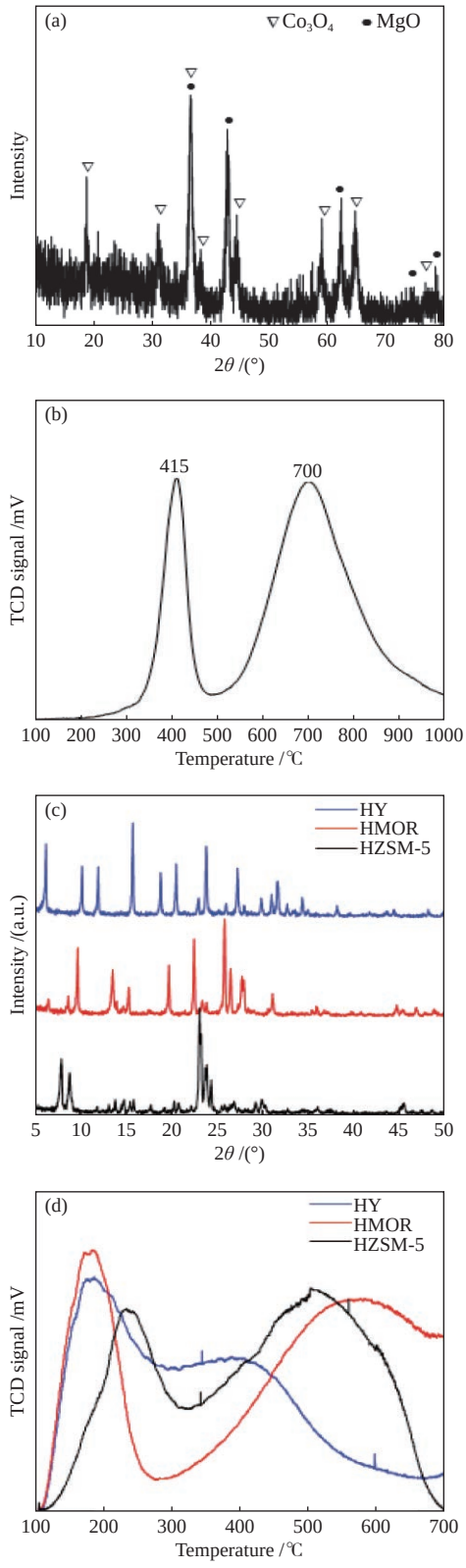

Figure 2 XRD pattern (a) and H_2-TPR profile (b) of the fresh Co-Mo/MgO catalyst, and XRD patterns (c) and NH_3-TPD profiles (d) of different zeolite catalysts profiles

2.2 Synthesis of CNTs by catalytic pyrolysis of SCB

2.2.1 Effect of zeolite type

Various types of zeolite catalysts including HZSM-5, HMOR, and HY with different porous structures and acidities are used for the pyrolysis of SCB at 500 °C to generate carbon-rich organic products. These pyrolysis products are decomposed and then deposited as solid CNMs on the surface of the Co-Mo/MgO catalyst. Generally, biomass vapors consist of carbon-containing compounds such as CO, CH_4, C_2H_4, benzene, and their derivatives that have been confirmed as efficient carbon sources for CNMs fabrication[49, 50]. Figure 3(a) and (b) shows the yields of pyrolysis products (gases, bio-oil, and biochar), as well as the yield of deposited carbon resulting from the catalytic pyrolysis of SCB using different zeolites. The total yield values of volatile products (bio-oil and gas) obtained by HY, HZSM-5, and HMOR zeolite catalysts are 34.4%, 32.8%, and 28.8%, respectively (Figure 3(a)). The variation in the activity of different zeolite catalysts is due to the difference in their acidic nature and porous structure. All types of the current zeolite catalysts have high acidity but with different porous structures. The HZSM-5 zeolite has a microporous structure with 10-membered rings pores in three-dimensions. Besides, HZSM-5 has two different types of elliptic channels (straight ones of 0.53 nm× 0.56 nm and sinusoidal ones of 0.51 nm× 0.55 nm), which bisect each other perpendicularly. However, the HY zeolite has a cubic structure with three-directional channels of 0.74 nm in diameter, whose intersections are “cages” with a diameter of 1.24 nm[51]. The porous structure of HY or HZSM-5 zeolite makes it suitable for the catalytic pyrolysis of SCB to generate volatile products. HMOR zeolite has an orthorhombic structure with 12-membered rings in a two-dimensional pore structure. The pore system of HMOR consists of main channels of 0.65 nm× 0.7 nm, which are connected by tortuous pores of 0.26 nm× 0.57 nm that form the so-called side pockets. The presence of these side pockets in HMOR may lead to a decrease in the catalytic pyrolysis activity and thus the formation of less volatile products than the other zeolite catalysts. On the other hand, the highest carbon yield (23.1%) is obtained by catalytic pyrolysis of SCB with HZSM-5 (Figure 3(b)). However, lower carbon yield values of 15.8% and 9.8% are produced using HMOR and HY pyrolysis catalysts, respectively.

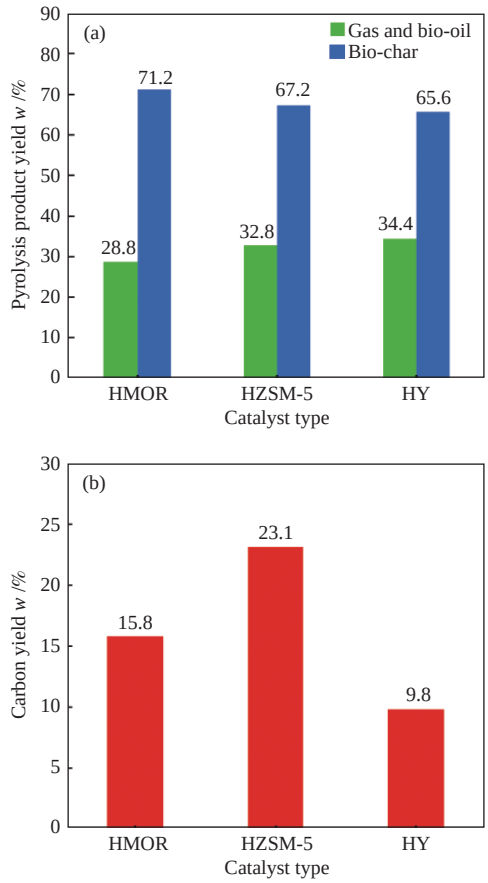

Figure 3　(a) Yields of pyrolysis products and (b) yield of deposited carbon obtained by SCB pyrolysis using various acidic zeolite catalysts

TEM analysis is used to study the morphological structure of the deposited carbon product. Figure 4 displays TEM images of CNMs obtained by catalytic pyrolysis of SCB using various zeolite catalysts. Bamboo-like MWCNTs are observed in all TEM images (Figure 4(a)−(f)). Also, CNTs are mainly produced along with a few CNOs by SCB pyrolysis with HZSM-5 (Figure 4(a) and (b)). However, a mixture of CNTs and CNOs is produced using HY and HMOR pyrolysis catalysts (Figure 4(c)−(f)). The outer diameters of CNTs observed in all TEM images were measured and displayed in the distribution histograms as shown in Figure 4. CNTs with a wide diameter distribution range (10−56 nm) are produced by bagasse pyrolysis with HZSM-5, while CNTs with smaller diameters are obtained in narrower ranges of 13−44 nm and 12−28 nm using HMOR and HY zeolite catalysts, respectively. In addition, the CNTs obtained by bagasse pyrolysis using the HY catalyst have the lowest average diameter (20 nm) compared to the other zeolite catalysts (27 nm).

Based on TEM observations, several CNMs are formed with different proportions according to the type

of zeolite catalyst, as illustrated in Figure 5. This may be due to the difference in the composition of the pyrolysis products generated by the effect of different zeolite catalysts. It was reported that HZSM-5 zeolite exhibited higher activity for aromatics production from a biomass source compared to HY and HMOR zeolites[52]. The HZSM-5 catalyst can remove oxygen from the oxygenated components in bio-oil through decarboxylation, dehydration, and decarbonylation reactions to produce aromatic hydrocarbons in addition to H_2O, CO, and CO_2[53 − 56]. Accordingly, the bio-oil obtained by HZSM-5 contains fewer oxygenated components and more aliphatic and aromatic hydrocarbons, which are more suitable for forming mainly CNTs with small and large diameters, along with a few CNOs (Figure 5(a)). Conversely, HMOR and HY catalysts have less selectivity for aromatics production, resulting in bio-oil formation with fewer aromatics and more oxygenates. Therefore, the volatile products generated by HY and HMOR catalysts are more suitable for the growth of both CNOs and CNTs (Figure 5(b)).

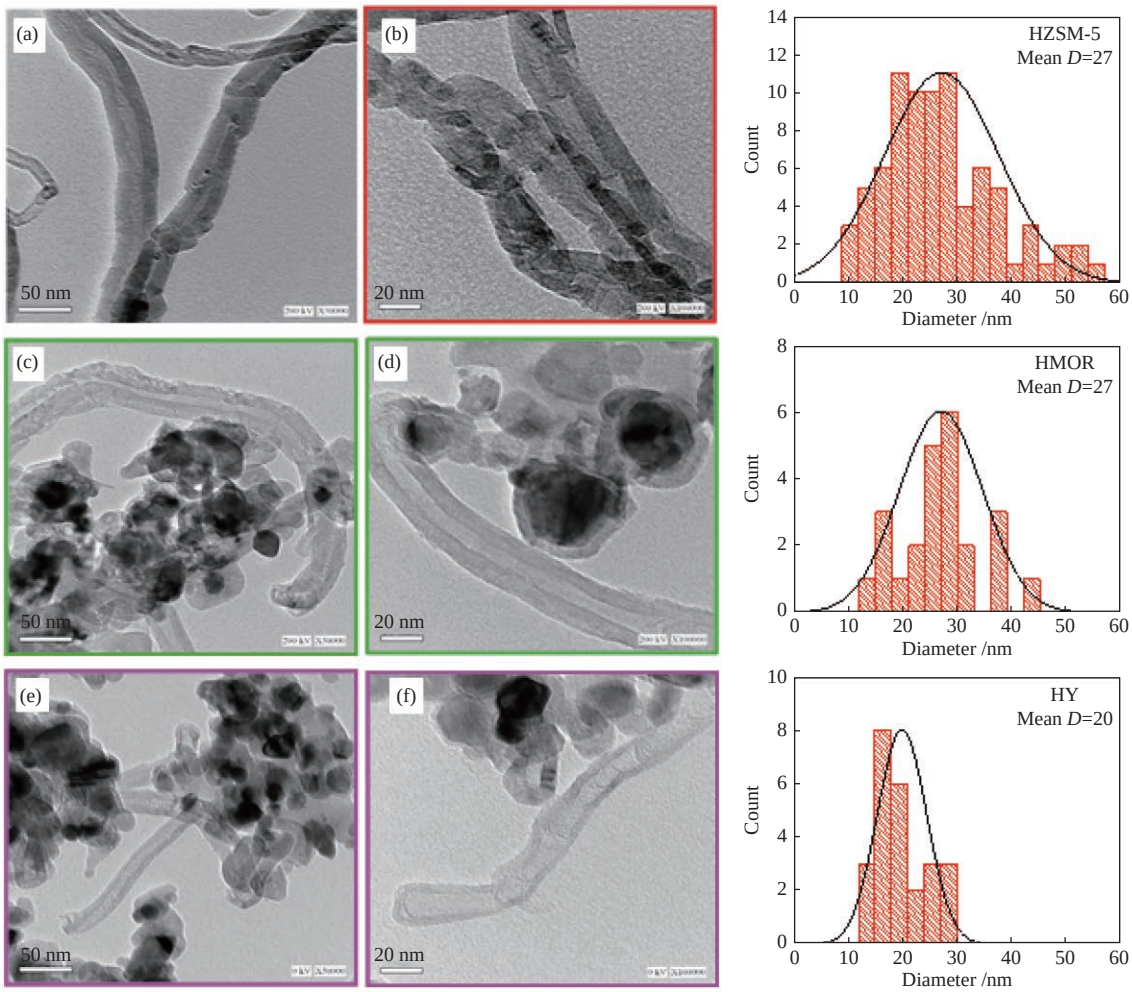

Figure 4 TEM images and outer diameter distribution histograms of CNMs obtained by SCB pyrolysis using different zeolites
(a), (b): HZSM-5, (c), (d): HMOR, and (e), (f): HY

Raman spectroscopy was used to monitor the quality, crystallinity, and purity of the produced CNMs. Figure 6 displays Raman spectra of the CNMs obtained by SCB pyrolysis using different zeolite catalysts. Generally, graphitic carbon material exhibits three Raman bands known as D, G, and 2D. The appearance of the D-band in the Raman spectra at about 1330 cm^{-1} suggests the presence of amorphous carbon or structural defects in the carbon nanostructure samples[57, 58]. The vibrations of the well-ordered carbon atoms mainly contribute to the appearance of the G-band at about 1565 cm^{-1}[59]. Besides, the presence of the 2D band at nearly 2675 cm^{-1} could refer to the purity of the carbon nanomaterials[60]. As shown in Figure 6, three characteristic bands (D, G, and 2D) are detected in the Raman spectrum of the carbon sample obtained via SCB pyrolysis with HZSM-5. However, only two Raman bands (D and G) are detected for the

corresponding CNMs obtained by using HMOR and HY zeolites. It was recognized that the I_D/I_G ratio can be used to monitor the degree of defects in CNMs, where a lower I_D/I_G value indicates fewer defects[61]. The values of I_D/I_G ratios for all samples of CNMs are presented in Figure 6. As depicted, high-quality CNTs with the lowest I_D/I_G value (0.70) are achieved using the HZSM-5 pyrolysis catalyst. It has been reported that the widths of all Raman bands (D, G, and 2D) correlate with the crystallinity of CNTs, where narrower bands refer to better crystal ordering[30]. In the present study, the sample synthesized via catalytic pyrolysis of SCB using HZSM-5 catalyst displays a narrower peak width compared to the other samples (Figure 6), indicating a better crystal ordering. These results agree well with the observations of TEM images. It can be inferred from all these results that CNTs with the highest yield and the best quality are produced by SCB pyrolysis using HZSM-5.

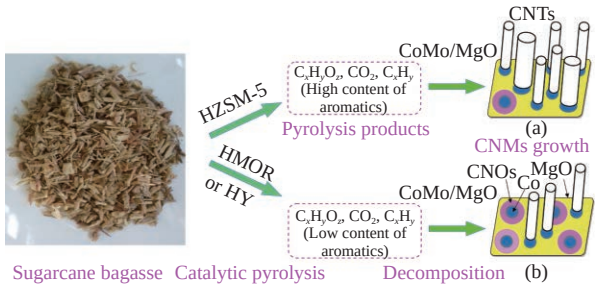

Figure 5　Schematic diagram for CNMs obtained over the Co-Mo/MgO catalyst via catalytic pyrolysis of SCB using various zeolite catalysts

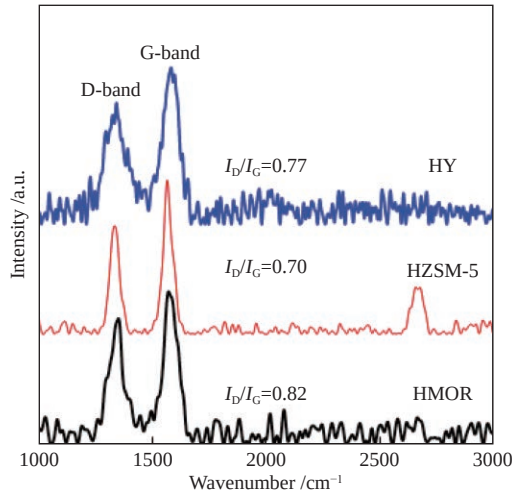

Figure 6　Raman spectra of CNMs obtained by catalytic pyrolysis of SCB using different zeolites

2.2.2　Effect of pyrolysis temperature

One of the most important factors affecting the generation of gas, liquid, and bio-char from biomass is the impact of pyrolysis temperature. In the present work, the effect of SCB pyrolysis at different temperatures on the yield of CNTs has been studied. The pyrolysis of SCB was carried out using HZSM-5 at temperatures ranging from 450 to 700 °C, while the nanocarbon product was formed at 700 °C over the Co-Mo/MgO catalyst. Figure 7(a) displays the yields of pyrolysis products obtained by SCB pyrolysis at various temperatures. It is evident that as the pyrolysis temperature rises, the bio-char yield decreases while the overall yield of gas and bio-oil increases. In detail, the yield of total gases and bio-oil increases from 32% to 40%, whereas the bio-char yield decreases from 68% to 60% by increasing the pyrolysis temperature from 450 to 700 °C, respectively. These results are due to the enhancement of SCB pyrolysis with HZSM-5 by increasing the pyrolysis temperature from 450 to 700 °C. Figure 7(b) shows the change in the yield of the deposited carbon product by changing the pyrolysis temperature of SCB. The carbon yield value increases sharply from 6.7% to reach the optimum value of 23.1% by raising the pyrolysis temperature from 450 to 500 °C, respectively. Thereafter, carbon yield decreases continuously to 16.7% through the successive increase in temperature up to 700 °C.

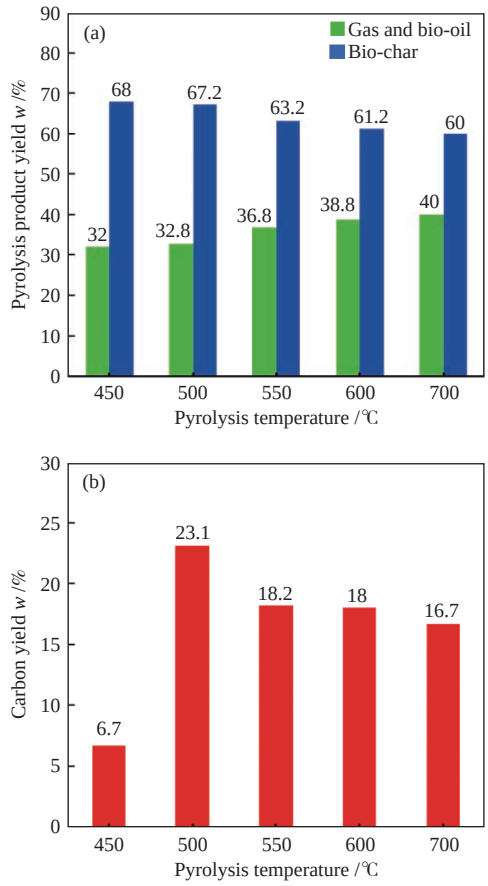

Figure 7　(a) Yields of pyrolysis products and (b) yield of deposited carbon obtained by catalytic pyrolysis of SCB at different temperatures using the SCB/ZSM-5 ratio of 12

Figure 8 shows TEM images of CNMs formed via catalytic pyrolysis of SCB at different temperatures. Clearly, pure BCNTs are produced at the pyrolysis temperature of 450 °C, while BCNTs and CNOs are formed at higher pyrolysis temperatures between 500 and 700 °C.

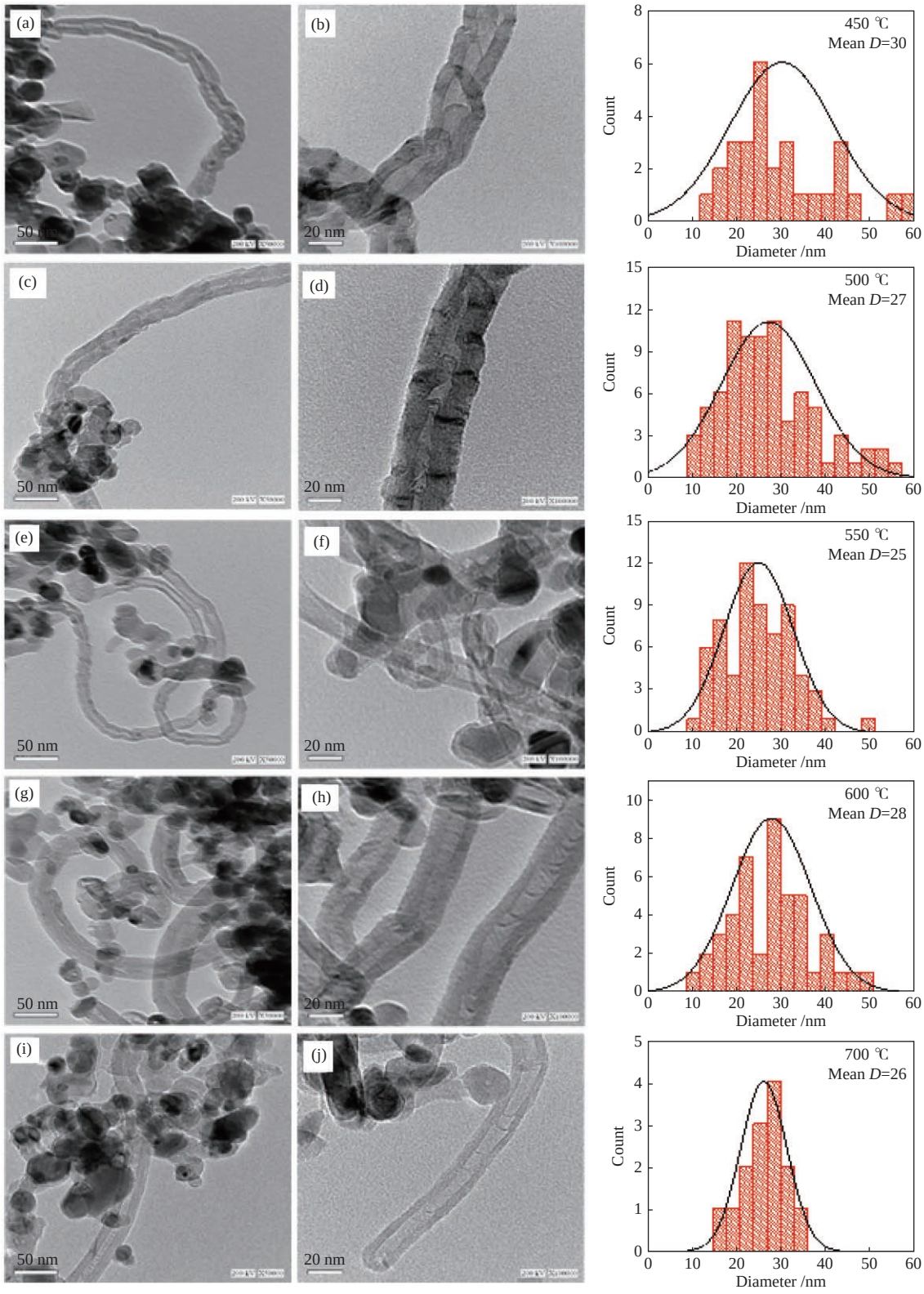

Figure 8 TEM images and outer diameter distribution histograms of CNMs synthesized by catalytic pyrolysis of SCB at different temperatures: (a), (b) 450 °C, (c), (d) 500 °C, (e), (f) 550 °C, (g), (h) 600 °C, and (i), (j) 700 °C

The proportion of CNOs increases by raising the pyrolysis temperature from 500 to 700 °C, while the proportion of CNTs decreases. Moreover, the formation of CNOs causes the encapsulation and deactivation of the catalyst particles, which explains the decrease in carbon yield by increasing the pyrolysis temperature from 500 to 700 °C (Figure 7(b)). We believe that the formation of CNOs in the solid carbon product is related to the proportion of CO_2 in the pyrolysis products. A large proportion of CO_2 can be produced at high pyrolysis temperatures, which may lead to oxidation of the active metal in the Co-Mo/MgO catalyst. It was reported that CNOs formation was attributed to the oxidation of cobalt particles by CO_2 during dry reforming of methane over the Co/MgO catalyst[62]. The distribution histograms of outer diameter CNTs obtained at various pyrolysis temperatures are also illustrated in Figure 8. The diameter range of CNTs becomes narrower by increasing the temperature from 450 to 700 °C.

Figure 9 displays the Raman spectra of as-grown CNMs obtained by catalytic pyrolysis of SCB at different temperatures. At temperatures between 450 and 600 °C, three known bands (D, G, and 2D) related to graphitic carbon materials appear in the Raman spectra. However, the sample obtained at pyrolysis temperature of 700 °C shows only D and G bands, revealing a low purity of CNMs. The I_D/I_G values for all carbon products are shown in Figure 9. The highest value of the I_D/I_G ratio (0.94) is achieved at the pyrolysis temperature of 450 °C, confirming the growth of CNMs with the lowest quality. However, the lowest I_D/I_G values (0.70 and 0.67) are obtained at 500 and 700 °C, suggesting the formation of CNMs with minimal defects.

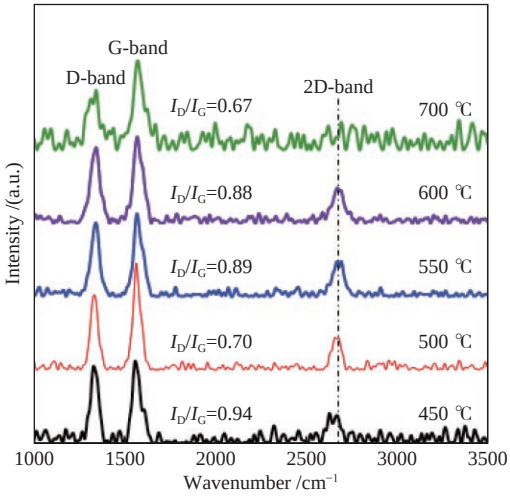

Figure 9　Raman spectra of CNMs obtained by catalytic pyrolysis of SCB at different temperatures

2.2.3　Synthesis of CNTs using various SCB/ZSM-5 ratios

Different amounts of SCB were pyrolyzed using a fixed amount of HZSM-5 zeolite to investigate the optimum biomass/zeolite ratio in terms of the CNTs yield. The catalytic pyrolysis of SCB was performed at 500 °C, while the growth of CNTs was carried out over the Co-Mo/MgO catalyst at 700 °C. Figure 10(a) and (b) shows the impact of the SCB/ZSM-5 ratio on the yields of both the pyrolysis products and the deposited nanocarbon product. As shown in Figure 10(a), the total yield of bio-oil and gases decreases from 36.4% to 32.8% by raising the SCB/ZSM-5 ratio from 3 to 12, while the yield of bio-char increases from 63.6% to 67.2%, respectively. This decrease in pyrolysis activity by increasing the ratio of SCB/ZSM-5 is due to reduced contact between the feedstock (SCB) and the used zeolite catalyst (HZSM-5). At high SCB/ZSM-5 ratios, the non-catalytic pyrolysis of bagasse is the predominant reaction that leads to increased bio-char formation. However, better contact between SCB and HZSM-5 active sites occurs at low SCB/ZSM-5 ratios, causing more gas and bio-oil products to be formed.

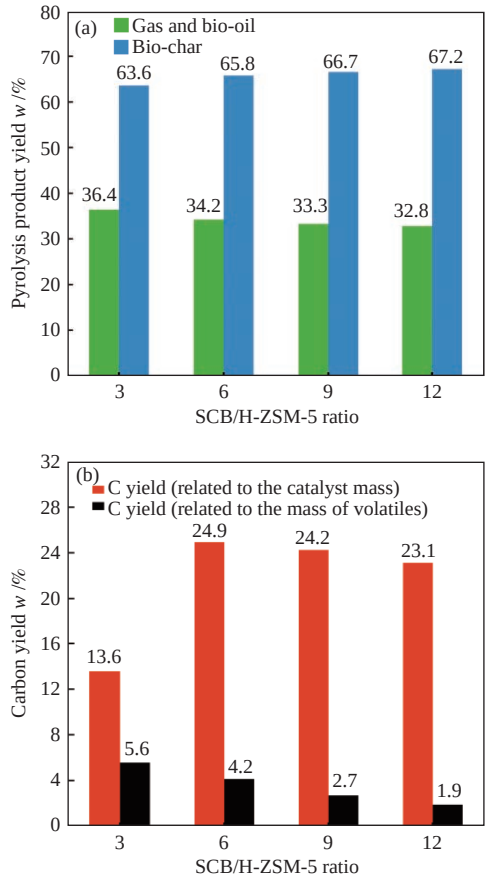

Figure 10　(a) Yields of pyrolysis products and (b) yield of deposited carbon obtained using various SCB/HZSM-5 ratios

It was published that the bio-char yield from the non-catalytic pyrolysis of SCB was higher than that from the catalytic pyrolysis with HZSM-5[63]. As shown in Figure 10(b), the carbon yield values were calculated according to the mass of the reduced Co-Mo/MgO catalyst, as well as the mass of the volatile products (gas and oil). The optimum value of the carbon yield calculated according to the mass of the catalyst is achieved using the SCB/ZSM-5 ratio of 6. However, the carbon yield value calculated based on the mass of volatile products decreases continuously by increasing the SCB/HZSM-5 ratio from 3 to 12.

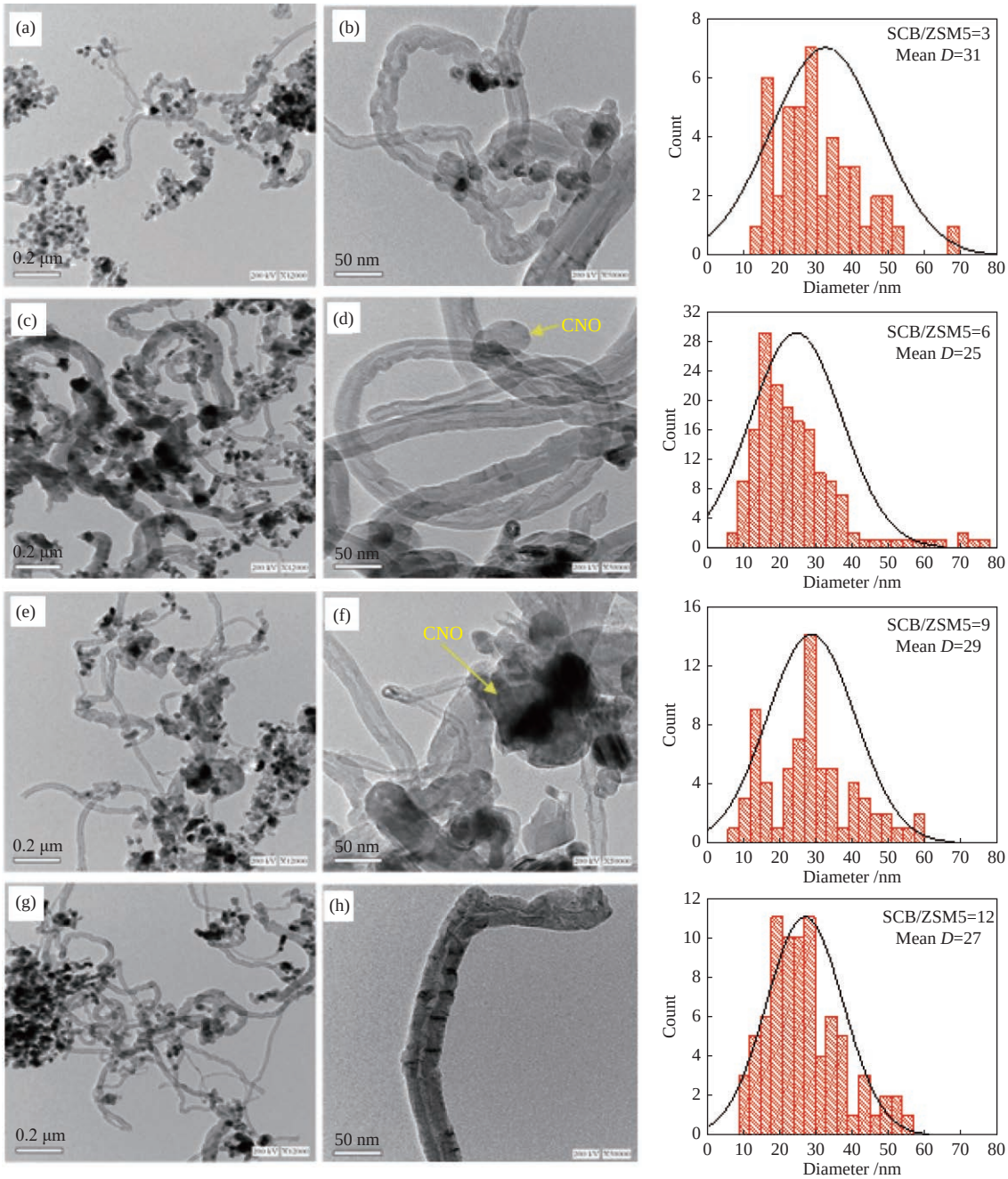

Figure 11 TEM images and outer diameter distribution histograms of CNTs obtained at different SCB/ZSM-5 ratios of: (a), (b) 3, (c), (d) 6, (e), (f) 9, and (g), (h) 12

Figure 11 displays TEM images of the carbon product obtained using various SCB/ZSM-5 ratios. CNTs are formed at all SCB/ZSM-5 ratios (Figure 11(a)−(h)). Using the lowest SCB/ZSM-5 ratio of 3, fewer CNTs are observed compared to the other samples (Figure 11(a)). Also, the produced CNTs have a wide diameter distribution range of 13−68 nm. By increasing the ratio to 6, dense CNTs of large and small diameters are produced (Figure 11(c)), indicating a higher growth activity of the Co-Mo/MgO catalyst for generating the

CNTs. Moreover, CNTs have the largest diameter distribution range of 7−76 nm. Using the SCB/ZSM-5 ratios of 9 and 12, CNTs with more uniform diameters are observed (Figure 11(e) and (f)). Also, the obtained CNTs have similar outer diameter distribution ranges of 7−58 and 10−56 nm, respectively. It can be concluded from the TEM observations that the SCB/ZSM-5 ratio of 6 is the best for the formation of dense CNTs with good quality.

Figure 12 displays the Raman spectra of the CNTs produced using different SCB/ZSM-5 ratios. For all nanocarbon samples, Raman spectra show three bands (D, G, and 2D) related to graphitic carbon materials. It is possible to track the purity of CNTs by calculating the I_{2D}/I_G ratio, where a greater I_{2D}/I_G ratio means better purity[61, 64]. The values of I_D/I_G and I_{2D}/I_G ratios are presented in Figure 12. The lowest I_D/I_G ratios (0.45 and 0.58) are achieved using SCB/ZSM-5 ratios of 3 and 6, indicating the formation of the best quality CNTs. On the other side, the CNTs produced using the SCB/ZSM-5 ratio of 6 display the greatest I_{2D}/I_G value (0.66), which means the growth of the CNTs with the highest purity. From these results, it can be concluded that the highest quality and best purity of CNTs can be produced using SCB/ZSM-5 ratios of 3 and 6.

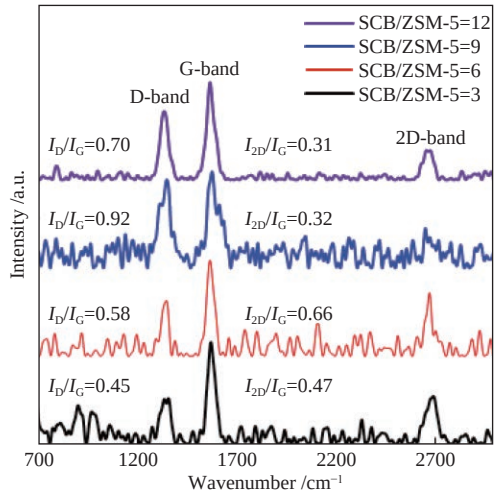

Figure 12　Raman spectra of CNTs obtained at different SCB/HZSM-5 ratios

3　Conclusions

The catalytic pyrolysis of SCB was studied using different zeolitic materials with various acidities and porous structures to investigate the best activity for the synthesis of CNTs using a two-stage process. The impact of pyrolysis temperature from 450 °C up to 700 °C on the yield and morphology of CNTs was also examined. It has been concluded that the yields of both CNTs and pyrolysis products (gas, bio-oil, and bio-char) are strongly influenced by zeolite type (HZSM-5, HMOR, and HY), pyrolysis temperature (450−700 °C), and SCB/ZSM-5 ratio (3−12). The results showed that the greatest yield of CNTs was achieved using HZSM-5 at the pyrolysis temperature of 500 °C and using the SCB/ZSM-5 ratio of 6. The largest yield of total bio-oil and gases (40%) was obtained at the pyrolysis temperature of 700 °C using the SCB/ZSM-5 ratio of 12. TEM analysis demonstrated the formation of pure BCNTs at low pyrolysis temperatures (450 °C) using the HZSM-5 catalyst, while CNTs and CNOs were produced at higher temperatures (500−700 °C). CNTs were produced with the largest diameter distribution range (7−76 nm) using the SCB/ZSM-5 ratio of 6, while the narrowest diameter distribution range (16−35 nm) was achieved with HZSM-5 at the pyrolysis temperature of 700 °C. Raman spectra proved the formation of CNTs with the highest quality and purity using SCB/ZSM-5 ratios of 3 and 6. This study revealed that the catalytic pyrolysis of SCB in a semi-batch reactor is an effective technique for producing high-quality CNTs. Small changes to the process and reactor can achieve better results. It is also possible to extend this work to other biomass resources.

References

[1] RAJA S, MATTOSO L H C, MOREIRA F K V. Biomass-Derived Nanomaterials. Nanostructured Materials for Energy Related Applications[M]. Cham: Springer Nature Switzerland AG, 2019: 243−270.

[2] TITIRICI M-M, WHITE R J, BRUN N, BUDARIN V L, SU D S, DEL MONTE F, CLARK J H, MACLACHLAN M J. Sustainable carbon materials[J]. Chem Soc Rev, 2015, **44:** 250−290.

[3] SHEN D, JIN W, HU J, XIAO R, LUO K. An overview on fast pyrolysis of the main constituents in lignocellulosic biomass to valued-added chemicals: Structures, pathways and interactions[J]. Renewable Suseamable Energy Rev, 2015, **51**(6): 761−774.

[4] PATRA T K, SHETH P N. Biomass gasification coupled with producer gas cleaning, bottling and HTS catalyst treatment for H2-rich gas production[J]. Int J Hydrogen Energy, 2019, **44:** 11602−11616.

[5] BASU P. Biomass Gasification, Pyrolysis and Torrefaction: Practical Design and Theory[M]. Amsterdam: Elsevier, 2018.

[6] REZAEI P S, SHAFAGHAT H, DAUD W M A W. Production of green aromatics and olefins by catalytic cracking of oxygenate compounds derived from biomass pyrolysis: A review [J]. Appl Catal A: Gen, 2014, **469:** 491−511.

[7] CHA J S, PARK S H, JUNG S C, RYU C, JEON J K, SHIN M C, PARK Y K. Production and utilization of biochar: A review[J]. J Ind Eng

Chem, 2016, **40:** 1−15.
[8] QIAN K, KUMAR A, ZHANG H, BELLMER D, HUHNKE R. Recent advances in utilization of biochar[J]. Renewable Sustainable Energy Rev, 2015, **42:** 1055−1064.
[9] VERMA D, GOPE P C, SINGH I, JAIN S. Processing and Properties of Bagasse Fibers. Biomass and Bioenergy: Processing and Properties. [M], Springer International Publishing, 2014: 63-75.
[10] GARCA-PÈREZ M, CHAALA A, ROY C. Vacuum pyrolysis of sugarcane bagasse[J]. J Anal Appl Pyrolysis, 2002, **65:** 111−136.
[11] DRUMMOND A R F, DRUMMOND I W. Pyrolysis of sugar cane bagasse in a wire-mesh reactor[J]. Ind Eng Chem Res, 1996, **35:** 1263−1268.
[12] FRAGA-ARAUJO A R. Pyrolytic decomposition of lignocellulosic materials[D]. London: Imperial College, University of London, 1990.
[13] SARANGI D, HIEROLD C, KARIMI A. Carbon nanotubes over metallic wires and its possible applications[J]. Fullerenes, Nanotub, Carbon Nanostruct, 2005, **13:** 243−254.
[14] POUDEL YR, LI W. Synthesis, properties, and applications of carbon nanotubes filled with foreign materials: A review[J]. Mater Today Phys, 2018, **7:** 7−34.
[15] XIE X, GAN T, SUN D, WU K. Application of multi - walled carbon nanotubes/nafion composite film in electrochemical determination of Pb^{2+}[J]. Fullerenes, Nanotub, Carbon Nanostruct, 2008, **16:** 103−13.
[16] HARRIS P J F. Carbon Nanotube Science: Synthesis, Properties and Applications [M]. Cambridge: Cambridge University Press, 2009.
[17] MAZOV I N, RUDINA N A, ISHCHENKO A V., KUZNETSOV V L, ROMANENKO A I, ANIKEEVA O B, SUSLYAEV V I, ZHURAVLEV V A. Structural and physical properties of MWNT/polyolefine composites[J]. Fullerenes, Nanotub, Carbon Nanostructures, 2012, **20:** 510−518.
[18] ROSLAN M S, CHAUDARY K T, HAIDER Z, AZIZ M S, ALI J. Multi-walled carbon nanotubes grow under low pressure hydrogen, air, and argon ambient by arc discharge plasma[J]. Fullerenes, Nanotub, Carbon Nanostructures, 2017, **25:** 269−272.
[19] CHRZANOWSKA J, HOFFMAN J, MAŁOLEPSZY A, MAZURKIEWICZ M, KOWALEWSKI T A, SZYMANSKI Z, STOBINSKI L. Synthesis of carbon nanotubes by the laser ablation method: Effect of laser wavelength[J]. Phys Status Solidi, 2015, **252:** 1860−1867.
[20] AWADALLAH A E, ABDEL-HAMID S M, EL-DESOUKI D S, ABOUL-ENEIN A A, ABOUL-GHEIT A K. Synthesis of carbon nanotubes by CCVD of natural gas using hydrotreating catalysts[J]. Egypt J Pet, 2012, **21:** 101−107.
[21] SHUKRULLAH S, MOHAMED N M, SHAHARUN M S, NAZ M Y. Mass production of carbon nanotubes using fluidized bed reactor: A Short review[J]. Trends Appl Sci Res, 2014, **9:** 121−131.
[22] KUMAR M, ANDO Y. Chemical vapor deposition of carbon nanotubes: A review on growth mechanism and mass production[J]. J Nanosci Nanotechnol, 2010, **10:** 3739−58.
[23] AWADALLAH A E, ABDEL-MOTTALEB M S, ABOUL-ENEIN A A, YONIS M M, ABOUL-GHEIT A K. Catalytic decomposition of natural gas to CO/CO_2-free hydrogen production and carbon nanomaterials using MgO-supported monometallic iron family catalysts[J]. Chem Eng Commun, 2015, **202:** 163−74.
[24] AWADALLAH A E, ABOUL-ENEIN A A, EL-DESOUKI D S, ABOUL-GHEIT A K. Catalytic thermal decomposition of methane to CO_x-free hydrogen and carbon nanotubes over MgO supported bimetallic group VIII catalysts[J]. Appl Surf Sci, 2014, **296:** 100−107.
[25] AWADALLAH A E, AHMED W, NOOR EL-DIN M R, ABOUL-ENEIN A A. Novel aluminosilicate hollow sphere as a catalyst support for methane decomposition to CO <inf>x</inf> -free hydrogen production[J]. Appl Surf Sci, 2013, **287:** 415−422.
[26] CHEN F, WU C, DONG L, VASSALLO A, WILLIAMS P T, HUANG J. Characteristics and catalytic properties of $Ni/CaAlO_x$ catalyst for hydrogen-enriched syngas production from pyrolysis-steam reforming of biomass sawdust[J]. Appl Catal B: Environ, 2016, **183:** 168−175.
[27] LIU W J, TIAN K, HE Y R, JIANG H, YU H Q. High-yield harvest of nanofibers/mesoporous carbon composite by pyrolysis of waste biomass and its application for high durability electrochemical energy storage[J]. Environ Sci Technol, 2014, **48:** 13951−13959.
[28] THOMPSON E, DANKS A E, BOURGEOIS L, SCHNEPP Z. Iron-catalyzed graphitization of biomass[J]. Green Chem, 2015, **17:** 551−556.
[29] BERND M G S, BRAGANÇA S R, HECK N, FILHO LCPDS. Synthesis of carbon nanostructures by the pyrolysis of wood sawdust in a tubular reactor[J]. J Mater Res Technol, 2017, **6:** 171−177.
[30] ALVES J O, ZHUO C, LEVENDIS Y A, TENÓRIO J A S. Catalytic conversion of wastes from the bioethanol production into carbon nanomaterials[J]. Appl Catal B: Environ, 2011, **106:** 433−444.
[31] ABOUL-ENEIN A A, ARAFA E I, ABDEL-AZIM S M, AWADALLAH A E. Synthesis of multiwalled carbon nanotubes from polyethylene waste to enhance the rheological behavior of lubricating grease[J]. Fullerenes, Nanotub, Carbon Nanostructures, 2020. Doi: 10.1080/1536383X.2020.1806828.
[32] ABOUL-ENEIN A A, AWADALLAH A E. Impact of Co/Mo ratio on the activity of CoMo/MgO catalyst for production of high-quality multi-walled carbon nanotubes from polyethylene waste[J]. Mater Chem Phys, 2019, **238:** 121879.
[33] ABOUL-ENEIN A A, AWADALLAH A E. Production of nanostructured carbon materials using Fe-Mo/MgO catalysts via mild catalytic pyrolysis of polyethylene waste[J]. Chem Eng J, 2018, **354:** 802−816.
[34] INFANTES-MOLINA A, MÉRIDA-ROBLES J, RODRÍGUEZ-CASTELLÓN E, PAWELEC B, FIERRO JLG, JIMÉNEZ-LÓPEZ A. Catalysts based on Co/zirconium doped mesoporous silica MSU for the hydrogenation and hydrogenolysis/hydrocracking of tetralin[J]. Appl Catal A: Gen, 2005, **286:** 239−248.
[35] AWADALLAH A E, ABOUL-ENEIN A A. Catalytic decomposition of methane to CO_x-free hydrogen and carbon nanotubes over Co-W/MgO catalysts[J]. Egypt J Pet, 2015, **24:** 299−306.
[36] AWADALLAH A E, ABOUL-ENEIN A A, ABOUL-GHEIT A K. Impact of group VI metals addition to Co/MgO catalyst for non-oxidative decomposition of methane into CO_x-free hydrogen and carbon nanotubes[J]. Fuel, 2014, **129:** 27−36.
[37] TUTI S, PEPE F. On the catalytic activity of cobalt oxide for the steam reforming of ethanol[J]. Catal lett, 2008, **122:** 196−203.

[38] MILLER J E, JACKSON N B, EVANS L, SAULT A G, GONZALES M M. The formation of active species for oxidative dehydrogenation of propane on magnesium molybdates[J]. Catal Lett, 1999, **58:** 147−152.
[39] ABOUL-ENEIN A A, AWADALLAH A E. A novel design for mass production of multi-walled carbon nanotubes using Co-Mo/MgO catalyst via pyrolysis of polypropylene waste: Effect of operating conditions[J]. Fullerenes, Nanotub, Carbon Nanostructures, 2018, **26:** 591−605.
[40] ABOUL-FOTOUH S M K, ALI L I, NAGHMASH M A, ABOUL-GHEIT N A K. Effect of the Si/Al ratio of HZSM-5 zeolite on the production of dimethyl ether before and after ultrasonication[J]. Fuel Chem Technol, 2017, **45**(5): 581−588.
[41] AWADALLAH A E, EL-DESOUKI D S, ABOUL-GHEIT N A K, IBRAHIM A H, ABOUL-GHEIT A K. Effect of crystalline structure and pore geometry of silica based supported materials on the catalytic behavior of metallic nickel particles during methane decomposition to CO_x-free hydrogen and carbon nanomaterials[J]. Int J Hydrogen Energy, 2016, **41:** 16890−902.
[42] TRAVKINA O S, AGLIULLIN M R, FILIPPOVA N A, KHAZIPOVA A N, DANILOVA I G, GRIGOR'EVA N G, NARENDER N, PAVLOV M L, KUTEPOV B I. Template-free synthesis of high degree crystallinity zeolite y with micro-meso-macroporous structure[J]. RSC Adv, 2017, **7:** 32581−32590.
[43] KATADA N, IGI H, KIM J H, NIWA M. Determination of the acidic properties of zeolite by theoretical analysis of temperature-programmed desorption of ammonia based on adsorption equilibrium[J]. J Phys Chem B, 1997, **101:** 5969−5677.
[44] WEBER R W, MÖLLER K P, O'CONNOR C T. The chemical vapour and liquid deposition of tetraethoxysilane on ZSM-5, mordenite and beta[J]. Microporous Mesoporous Mater, 2000, **35–36:** 533−543.
[45] CHU S, YANG L, GUO X, DONG L, CHEN X, LI Y, MU X. The influence of pore structure and Si/Al ratio of HZSM-5 zeolites on the product distributions of A-cellulose hydrolysis[J]. Mol Catal, 2018, **445:** 240−247.
[46] GAO Y, ZHENG B, WU G, MA F, LIU C. Effect of the Si/Al ratio on the performance of hierarchical ZSM-5 zeolites for methanol aromatization[J]. RSC Adv, 2016, **6:** 83581−83588.
[47] KOUVA S, KANERVO J, SCHÜSSLER F, OLINDO R, LERCHER JA, KRAUSE O. Sorption and diffusion parameters from vacuum-TPD of ammonia on H-ZSM-5[J]. Chem Eng Sci, 2013, **89:** 40−48.
[48] LÜ J, ZHOU S, MA K, MENG M, TIAN Y. The effect of P modification on the acidity of HZSM-5 and P-HZSM-5/CuO-ZnO-Al_2O_3 mixed catalysts for hydrogen production by dimethyl ether steam reforming[J]. Chin J Catal, 2015, **36:** 1295−1303.
[49] PRASEK J, DRBOHLAVOVA J, CHOMOUCKA J, HUBALEK J, JASEK O, ADAM V, KIZEK R. Methods for carbon nanotubes synthesis—review[J]. J Mater Chem, 2011, **21:** 15872.
[50] DEBALINA B, REDDY RB, VINU R. Production of carbon nanostructures in biochar, bio-oil and gases from bagasse via microwave assisted pyrolysis using Fe and Co as susceptors[J]. J Anal Appl Pyrolysis, 2017, **124:** 310−318.
[51] RABO J A. Zeolite Chemistry and Catalysis, Acs Monograph No 171 [M], Washington , DC: *ACS*, 1976.
[52] MIHALCIK D J, MULLEN C A, BOATENG A A. Screening acidic zeolites for catalytic fast pyrolysis of biomass and its components[J]. J Anal Appl Pyrolysis, 2011, **92:** 224−232.
[53] RAHMAN M M, LIU R, CAI J. Catalytic fast pyrolysis of biomass over zeolites for high quality bio-oil – A review[J]. Fuel Process Technol, 2018, **180:** 32−46.
[54] WANG K, KIM K H, BROWN R C. Catalytic pyrolysis of individual components of lignocellulosic biomass[J]. Green Chem, 2014, **16:** 727−735.
[55] WANG K, BROWN R C. Catalytic pyrolysis of corn dried distillers grains with solubles to produce hydrocarbons[J]. ACS Sustainable Chem Eng, 2014, **2:** 2142−2148.
[56] VICHAPHUND S, AHT-ONG D, SRICHAROENCHAIKUL V, ATONG D. Catalytic upgrading pyrolysis vapors of jatropha waste using metal promoted ZSM-5 catalysts: An analytical PY-GC/MS[J]. Renewable Energy, 2014, **65:** 70−77.
[57] DRESSELHAUS M S, DRESSELHAUS G, SAITO R, JORIO A. Raman spectroscopy of carbon nanotubes[J]. Phys Rep, 2005, **409:** 47−99.
[58] DRESSELHAUS M S, JORIO A, HOFMANN M, DRESSELHAUS G, SAITO R. Perspectives on carbon nanotubes and graphene Raman spectroscopy[J]. Nano Lett, 2010, **10:** 751−758.
[59] GONG J, LIU J, WAN D, CHEN X, WEN X, MIJOWSKA E, JIANG Z, WANG Y, TANG T. Catalytic carbonization of polypropylene by the combined catalysis of activated carbon with Ni_2O_3 into carbon nanotubes and its mechanism[J]. Appl Catal A: Gen, 2012, **449:** 112−120.
[60] DILEO R A, LANDI B J, RAFFAELLE R P. Purity assessment of multiwalled carbon nanotubes by Raman spectroscopy[J]. J Appl Phys, 2007, **101:** 64307−64312.
[61] YAO D, ZHANG Y, WILLIAMS P T, YANG H, CHEN H. Co-production of hydrogen and carbon nanotubes from real-world waste plastics: Influence of catalyst composition and operational parameters[J]. Appl Catal B: Environ, 2018, **221:** 584−597.
[62] LI J, LI J, ZHU Q. Carbon deposition and catalytic deactivation during CO_2 reforming of CH_4 over Co/MgO catalyst[J]. Chin J Chem Eng, 2018, **26:** 2344−2350.
[63] FARAHEEN KABIR AHMAD S, FAZARA MD ALI U, MD ISA K, RAHAYU MOHAMED A, SATAIMURTHI O. Comparative performance of catalytic and non-catalytic pyrolysis of sugarcane bagasse in catatest reactor system [C]// IOP Conference Series: Materials science and engineering. London: Institute of Physics Publishing, 2020: 012069.
[64] ABOUL-ENEIN A A, SOLIMAN F S, BETIHA M A. Co-production of hydrogen and carbon nanomaterials using NiCu/SBA15 catalysts by pyrolysis of a wax by-product: Effect of Ni-Cu loading on the catalytic activity[J]. Int J Hydrogen Energy, 2019, **44:** 31104−31120.

沸石催化甘蔗渣裂解制备多壁碳纳米管

ABOUL-ENEIN Ateyya A.[1,2,*]，AWADALLAH Ahmed E.[1,2]，
EL-DESOUKI Doaa S.[1]，ABOUL-GHEIT Noha A.K.[1]

（1. Process Development Division, Egyptian Petroleum Research Institute, Cairo 11727, Egypt;
2. EPRI-Nanotechnology Center, Egyptian Petroleum Research Institute, Cairo 11727 , Egypt）

摘 要: 通过催化热解农业废弃物甘蔗渣 (SCB), 采用两步工艺生产具有显著应用价值的碳纳米管 (CNTs)。主要研究沸石催化剂 (HZSM-5、HMOR 和 HY)、热解温度 (450−700 ℃) 和 SCB/ZSM-5 的比例 (3−12) 对 SCB 催化热解的影响, 确定最佳工艺参数。随后, 将第一步产生富含碳的热解产物用于第二步由 Co-Mo/MgO 催化生长 CNTs。通过简单的两步工艺催化热解 SCB 生产 CNTs。SCB 的催化热解在半间歇式反应器 (外径 = 4 cm, 长度 = 90 cm) 中进行, CNTs 的生长在水平反应器 (外径 = 2.5 cm, 长度 = 100 cm) 中进行。两个反应器通过玻璃管 (直径 0.6 cm, 长度 12 cm) 连接并将热解产物从反应器 I 转移到反应器 II。在半间歇式反应器中放入经过预处理的 SCB 和沸石催化剂, 并以 20 ℃/min 加热到反应所需温度。随后, 将 0.5 g Co-Mo/MgO 加入到水平反应器中作为 CNTs 的生长催化剂。在一个典型的实验中, 将 2 g 沸石催化剂、24 g SCB 放入半间歇式反应器, 研究了不同种类沸石催化剂在 500 ℃ 温度条件下对 SCB 热解的影响。接着, 使用 HZSM-5 研究了不同温度 (450−700 ℃) 对 SCB 热解的影响。最后, 研究了不同 SCB/ZSM-5 投料比例 (SCB/ZSM-5 = 3、6、9、12) 对 SCB 热解的影响。此外, 水平反应器中的 CNTs 生长温度恒定为 700 ℃。通过 XRD、TPR 和 TPD 进行催化剂表征。XRD 谱图证实了催化剂存在 MgO 和 Co_3O_4, 以及以小尺寸颗粒形式存在的 $CoMoO_4$ 和 $MgMoO_4$。使用 XRD 数据根据 Scherrer 方程计算 45% Co-5% Mo/MgO 催化剂的平均晶粒尺寸为 25.8 nm。TPR 分析表明, Co-Mo/MgO 催化剂是由未反应的 Co_3O_4 以及混合氧化物组成。使用 XRD 数据, 计算得到 HZSM-5、HMOR 和 HY 的平均晶粒尺寸分别为 43、41 和 51 nm。NH_3-TPD 分析表明沸石催化剂存在大量的酸性位点。催化热解 SCB 结果表明, 由 HY 和 HZSM-5 催化剂在 500 ℃ 得到的挥发性产品 (生物油和气体) 的总收率值分别为 34.4% 和 32.8 %, 而使用 HMOR 产生的这些挥发性产品的收率值最低 (28.8%)。用 HZSM-5 催化热解 SCB 获得了最高的炭产量 (23.1%)。然而, 使用 HMOR 和 HY 热解催化剂产生的炭产量值较低, 分别为 15.8% 和 9.8%。使用 TEM 表征通过两步法生产的碳纳米管, 并且测量了 CNTs 的外径。数据显示, 用 HZSM-5 进行 SCB 热解产生了直径分布范围较宽的 CNTs (10−56 nm), 而用 HMOR 和 HY 热解催化剂则分别获得了直径较窄的 CNTs (13−44 nm, 12−28 nm)。拉曼光谱分析表明, 使用 HZSM-5 作为 SCB 热解的催化剂可以生产最优的 CNTs。研究了不同热解温度对 CNTs 产量的影响。结果显示, 将热解温度从 450 ℃ 提高到 500 ℃, 炭产率值从 6.7% 达到最佳值 23.1%, 接着增加温度至 700 ℃, 炭产量下降至 16.7%。随后对不同温度下催化热解形成的炭产品进行 TEM 表征, 结果显示, 随着温度的升高炭产品中 CNTs 的比例下降, CNTs 的直径范围变窄。拉曼光谱分析结果表明, 在 500 和 700 ℃ 形成的 CNMs 具有最少的缺陷。研究了投料比例对炭产品产量的影响, 结果表明, SCB/ZSM-5 的比例从 3 提高到 12, 生物油和气体的总产量从 36.4% 下降到 32.8%, 而生物炭的产量分别从 63.6% 增加到 67.2%。根据催化剂的质量计算得到炭产量的最佳值是使用 SCB/ZSM-5 比例为 6。使用 TEM 表征不同投料比例生产的炭产品, 分析表征结果可得 SCB/ZSM-5 的比例为 6, 是形成具有良好质量的致密 CNTs 的最佳选择。并且不同投料比例的拉曼光谱显示, SCB/ZSM-5 比例为 6 可以生产最优的 CNTs。沸石类型 (HZSM-5、HMOR 和 HY)、热解温度 (450−700 ℃) 和 SCB/ZSM-5 比例 (3−12) 影响 CNTs 和热解产物 (气体、生物油和生物炭) 的产量。实验结果表明, 获得最高 CNTs 产量的条件为: 热解温度为 500 ℃、SCB/ZSM-5 比例为 6; 获得最高生物油和气体总产量 (40%) 的条件为: 热解温度为 700 ℃、SCB/ZSM-5 比例为 12。TEM 分析表明, 使用 HZSM-5 催化剂在热解温度 450 ℃ 只生成竹节状碳纳米管 (BCNTs), 而 CNTs 和碳纳米洋葱 (CNO) 是在较高温度热解温度 (500−700 ℃) 下产生的。使用 SCB/ZSM-5 的比例为 6 时, 生成 CNTs 的直径分布范围最大 (7−76 nm)。拉曼光谱分析表明, 使用 SCB/ZSM-5 的比例为 6 时, 形成的 CNTs 最优。该研究显示, 在半间歇式反应器中催化热解 SCB 是生产 CNTs 的有效技术, 通过对工艺和反应器的优化可以达到更好的效果。

关键词: 碳纳米管; Co-Mo/MgO; 热解; 甘蔗渣; ZSM-5 沸石

中图分类号: O643.3 **文献标识码:** A